White paper:

Lake and fjord metabolism

WateriTech
Døjsøvej 1, 8660 Skanderborg, Denmark
Web: www.wateritech.com
CVR: 40272860

February 2025

VERSION: 1.1
DATE: 23. February 2025
AUTHORS: Dennis Trolle, Anders Nielsen and Christopher S. Nielsen
CITE AS: Trolle, D., Nielsen, A. and Nielsen, C.S. 2025. Lake and fjord metabolism. WateriTech white paper v1.1, 18p.

Content

Background

Aquatic ecosystem metabolism refers to the ecosystem-scale rates of organic matter cycling in aquatic ecosystems - namely gross primary production (GPP) and ecosystem respiration (ER) - that form the base of food webs and influence biogeochemical cycling rates (Jankowski et al. 2021). From a management perspective, ecosystem metabolism is interesting as GPP and ER responds to environmental change and disturbances in streams, lakes, wetlands, as well as estuaries (Hoellein et al. 2013), and can therefore be used as indicators of the ecosystem's health status. Metabolism can be derived from diurnal variations in dissolved oxygen (DO) concentrations based on in-situ sensor measurements. Historically, the cost and level of accuracy of oxygen sensors have limited the widespread application of metabolism. However, recent advances in sensor and modelling technologies now enable routine monitoring of dissolved oxygen (DO) at high quality and low cost, and real-time modelling of aquatic ecosystem function (GPP and ER), including the influence of key physical processes such as gas exchange with the atmosphere. WateriTech has developed a new inverse modelling approach, combining real-time sensor monitoring with machine learning (differential evolution), to deliver cost effective estimates of aquatic metabolism. The method has been tailored for stratifying (lakes and fjords) and vertically mixed (streams) water bodies, respectively. This white paper describes the key concept for deriving metabolism in stratifying lakes and fjords.

About WateriTech & WaterWebTools

WateriTech is a research and consultancy company founded in 2019 by world leading researchers within water quality modelling and data analytics. The company is based in Denmark but offer its services and solutions globally. WateriTech specializes in the development and application of open source hydrological and ecological models, IoT sensor monitoring and advanced data analytics, and focus on digital solutions for addressing water quality, flooding and drought challenges. WateriTech and partners have developed the highly recognized WaterWebTools platform, which is a user-friendly web-platform for live streaming, quality control and postprocessing of sensor data, as well as operationalization of hydrological and water quality models for forecasting purposes. The WaterWebTools platform, which also allows transmission of data to customers own data platform or 3. party platforms, is widely used in Denmark and across Europe by the municipal and water utility sectors, private companies as well as research institutions.

Introduction

The primary drivers of ecosystem metabolism include temperature, light, hydrology, and the quantity and quality of organic matter and nutrients (Battin et al. 2023; Caffrey 2004; Solomon et al. 2013). Metabolic rates can be derived based on different approaches, including isotope analysis, in-situ incubation experiments, field campaigns for monitoring the mass balance of carbon, and sensor technology. Advances in sensor technology during the past 10 years, including improved accuracy and stability and lower cost, has enabled a more widespread use of this approach for deriving metabolism (Hall and Hotchkiss 2017). Using one of more sensors installed in-situ, water temperature and oxygen concentration is measured in high frequency (typically 10-30 minute intervals). Using a process-based model that is calibrated to the daily variation in oxygen concentrations, GPP and ER can be estimated for each single day. The method developed by WateriTech is inspired partly by the approaches described by Staehr et al. (2012), Obrador et al. (2014) and Giling et al. (2017), with several new advances, including advanced qa/qc routines for cleaning sensor data, improved thermocline processing, more accurate numerical integration, use of differential evolution for model parameter optimization, parameter uncertainty estimation, parallel processing of model runs for large datasets, and operationalization of the model via the WaterWebTools portal.

Data collection

When estimating metabolism in stratifying lakes and fjords, vertical profiles of subdaily (e.g., 15 min intervals) water temperature and DO are required. WateriTech produces data buoys for this specific purpose (Fig. 1), but data from 3. party can also be linked to the WaterWebTools platform, thereby enabling metabolism estimates for any location on the planet.

Fig. 1. Example of a data buoy (left) produced by WateriTech. Here, several OPTOD optical oxygen and temperature sensors (right) are placed at fixed depths, where the number of sensors and their placement is adapted to the individual system.

Besides in-situ sensor data, local data for incoming radiation, wind speed and barometric pressure is also required. By default, WaterWebTools will automatically harvest local data from the ERA5 gridded weather product, which is available globally in near real-time and hourly temporal resolution, and for spatial grids of approx. 30 km spacing. Time series of Secchi depth can also be utilized or alternatively estimated from a cosine seasonal function, and is used to derive photosynthetic active radiation (PAR) as a function of depth and time.

Data pre-processing

A series of pre-processing steps are first conducted to format raw sensor data and weather data into quality assured and quality controlled equidistant time series.

Data cleaning and control

To achieve adequate quality of the in-situ collected data prior to metabolism processing, the raw sensor data is initially harmonized with respect to sampling frequency to create an equidistant time series followed by filtering on sensor-specific error values. Hereafter, outliers are detected with a modified version of the SentemQC approach by van't Veen et al. (2025), which identifies and marks anomalies in the dataset using successive moving windows with varying window sizes. This method has proved efficient for cleaning sensor data, not only for identifying individual outliers, but also clusters of anomalies.

Data resampling and interpolation

After cleaning and control the data is processed further with resampling into half hourly intervals, and then smoothed using a 4-hour running window. These steps are based on experiences and recommendations from the scientific literature, including Staehr et al. (2012), Obrador et al. (2014) and Giling et al. (2017). Hereafter, data is interpolated to a user defined depth grid that represents the waterbody.

Weather and light data

Representative weather and light data are pre-processed according to the following steps:

- Download local weather data including incoming short wave radiation (E, W m^{-2}), wind speed (ws, m s^{-1}), and barometric pressure (P, kPa).
- Convert short wave radiation into photosynthetic active radiation at the surface (PAR_0, µmol m^{-2} s^{-1}), where:

  $PAR_0 = E * 4.6 * 0.45$ (Giling et al. 2017).
- Calculate Secchi depth (sd, m) for each day from cosine function (which reads maximum sd, minimum sd, and day of the year of maximum sd) or read this directly from external file
- Calculate light attenuation (KD, m^{-1}) from Secchi depth, where:

  $KD = 1.7 / sd$ (Giling et al. 2017)
- Derive PAR (µmol m^{-2} s^{-1}) for each layer depth (z) layer based on Secchi depth, where:

  $PAR(z) = PAR_0 \cdot e^{KD \cdot z}$ (Giling et al. 2017)
- Interpolate PAR to same depth grid and temporal resolution as sensor data.
- Interpolate wind speed and barometric pressure to same temporal resolution as sensor data.

Thermocline processing

The be able to take into account the effects of deepening of the surface mixed layer, and the effects of gas-exchange between the water and the atmosphere, when modelling oxygen concentrations and metabolism, the surface mixed layer depth and the bottom depth of the metalimnion must first be derived. When vertical temperature and density gradients are small, it can sometimes be difficult to detect these. WateriTech has therefore experimented with several different approaches for detecting these, including f.x. that typically used in metabolism studies of stratifying water bodies (e.g. Staehr et al. 2012, Obrador et al. 2014, Mziray et al. 2024). We have found that the piecewise linear segmentation algorithm described by Xu et al. (2019) is

generally the best and most stable at detecting mixed layer depth, thermocline depth, and the bottom depth of the thermocline. This approach is therefore used as a basis. In cases where this approach cannot detect mixed layer depth, we used the simple density gradient approach by Wilson et al. (2020) to estimate the mixed layer depth. In summary the steps for thermocline processing are:

- Calculate thermocline characteristics based on Xu et al. (2019) and Wilson et al. (2020) to identify surface mixed layer depth (Z_{mix}), and the bottom depth of the metalimnion (Z_{meta_lower}).
- If mixed layer depth is not detected by approach in Xu et al. (2019), use approach in Wilson et al. (2020). If thermocline is also not detected using approach by Wilson et al. (2020), assume that water column is fully mixed.
- Import hypsograph data and calculate layer areas and volumes for each depth grid.

Metabolism modelling

The main body of the metabolism model is a differential equation (Staehr et al. 2012), which describes the changes in oxygen concentration for each depth layer (i) due to gross primary production (GPP), ecosystem respiration (ER), the oxygen flux due to reaeration between the water surface and the atmosphere (Ds), the oxygen flux due to turbulence and diffusion (eddy diffusivity) (Dv), and the oxygen flux due to changes in mixing depth (Dz):

$$\frac{\Delta O_{2(i)}}{\Delta t} = GPP_i - ER_i - D_{s(i)} - D_{v(i)} + D_{z(i)}$$

To be able to solve this equation, each of these terms has to be derived for each individual layer.

Gross primary production

GPP (g O_2 m^{-3} h^{-1}) for each depth layer (i) is calculated based on approach in Song et al. (2016), and derived from $\mathbf{P_{max(i)}}$, the maximum photosynthetic rate (g O_2 m^{-3} h^{-1}) at saturating light for layer *i*, $\boldsymbol{\alpha(i)}$, the photosynthetic efficiency coefficient (g O_2 m^{-3} h^{-1} [µmol photons m^{-2} s^{-1}]$^{-1}$) for layer *i*, **temp(i)**, the water temperature (°C) of layer *i*, and θ_P, a temperature coefficient for primary production:

$$GPP_{(i)} = P_{max(i)} \cdot tanh\left(\frac{\alpha(i) \cdot PAR_{(z_i)}}{P_{max(i)}}\right) \cdot \theta_P{}^{(temp_i - 20)}$$

Where z_i is the depth (m) of layer *i*, and where the temperature coefficient (θ_P) is set to 1.036, as in Song et al. (2016). $P_{max(i)}$ and $\alpha(i)$ are two of the three parameters that are automatically calibrated by the model using a differential evolution algorithm.

Ecosystem respiration

The ecosystem respiration rate (ER) (g O_2 m^{-3} h^{-1}) is determined for each layer from $\mathbf{R_{20}}$, the respiration rate at 20°C (g O_2 m^{-3} h^{-1}), and $\boldsymbol{\theta_R}$, a coefficient for the thermal dependence of respiration:

$$\boldsymbol{ER_{(i)} = R_{20(i)} \cdot \theta_R^{(temp_i - 20)}}$$

Where a temperature coefficient (θ_R) of 1.073 is used, based on Jørgensen and Bendoricchio (2001). $R_{20(i)}$ is automatically calibrated by the model using a differential evolution algorithm.

Atmosphere-water gas exchange

Several approaches for estimating the gas exchange between the water surface and the atmosphere have been reported in the literature. To accommodate the strengths of different approaches, we derive the mean gas exchange from an ensemble of approaches. The flux of oxygen between the water and the atmosphere (Ds, g O_2 m^{-3} h^{-1}) is calculated as:

$$\boldsymbol{D_{s(i)} = \frac{K_{s,mean} \cdot (O_{2(i)} - O_{2sat(i)})}{Z_{mix}}}$$

Where $\mathbf{K_{s,mean}}$ is the mean gas exchange coefficient for oxygen (m h^{-1}), based on the average of an ensemble comprised of four empirical relations, and $\mathbf{O_{2sat}}$ is the oxygen concentration at saturation level at the given surface water temperature and barometric pressure (g O_2 m^{-3}).

The overall flux oxygen between water and atmosphere flux can be either positive (i.e. oxygen going into the water from the atmosphere, when water is undersaturated with oxygen) or negative (i.e. oxygen leaving the water due to supersaturation). The oxygen concentration at saturation level is derived from the approach in Song et al. (2016):

$$\boldsymbol{O_{2sat(i)} = e^{\left(-139.3441 + \frac{1575710}{temp(i)+273.15} - \frac{66423080}{(temp(i)+273.15)^2} + \frac{12438000000}{(temp(i)+273.15)^3} - \frac{862194900000}{(temp(i)+273.15)^4}\right)} \cdot \frac{Pa \cdot 0.998}{101.3}}$$

Where Pa is the barometric pressure (kPa).

The mean gas exchange coefficient ($K_{s,mean}$) is derived from the gas exchange velocity for a Schmidt number of 600 (K_{600}, m h^{-1}), and a temperature correction based on Raymond et al. (2012):

$$K_{s,mean} = K_{600,mean} \cdot \left(\frac{Sc}{600}\right)^{-0.5}$$

Where Sc is the dimensionless Schmidt number for the temperature of the surface layer, **temp(surf)** (derived from Raymond et al. 2012)**:**

$$Sc = 1568 - 86.04 \cdot temp(surf) + 2142 \cdot temp(surf)^2 - 0.0216 \cdot temp(surf)^3$$

$K_{600,mean}$ (m h^{-1}) is first calculated from four individual estimates of K_{600}, where **ws** is wind speed (m s^{-1}), and **LA** is lake area (km^2):

Vachon and Prairie (2013): $K_{600(1)} = \frac{(2.51 + 1.48 \cdot ws + 0.39 \cdot ws \cdot log10(LA))}{100}$

Cole and Caraco (1998): $K_{600(2)} = \frac{(2.07 + 0.215 \cdot ws^{1.7})}{100}$

Schilder et al. (2016): $K_{600(3)} = \frac{(0.9 + 0.97 \cdot ws)}{100}$

Crusius and Wanninkhof (2003): $K_{600(4)} = \frac{(0.168 + 0.228 \cdot ws^{2.2})}{100}$

Mean K_{600}: $K_{600,mean} = mean(K_{600(1)}, K_{600(2)}, K_{600(3)}, K_{600(4)})$

Turbulent diffusion

We have implemented two options for deriving the oxygen flux between layers driven by turbulent diffusion (eddy diffusivity). The first approach is based on Staehr et al. (2012), where the flux (Dv, g O_2 m^{-3} h^{-1}) is calculated from:

$$D_{v(i)} = \left[\frac{K_{v(i)} \cdot \left(O_{2(i)} - O_{2(i-1)}\right) + K_{v(i+1)} \cdot \left(O_{2(i)} - O_{2(i+1)}\right)}{h}\right] \cdot \frac{A_i}{V_i}$$

Where **$K_{v(i)}$** is the vertical turbulent diffusivity of layer *i*, **A_i** is the horizontal area (m^2) of the water column at layer *i* (derived from hypsograph), and **V_i** is the volume (m^3) of layer *i*.

Based on Staehr et al. (2012), and originally by Hondzo and Stefan (1993), $\mathbf{K_{v(i)}}$ can be estimated from the Brunt-Väisälä buoyancy frequency ($N^2_{(i)}$), which can be determined from the density gradient between water layers:

$$K_{v(i)} = 2.941 \cdot 10^{-3} \cdot (A_i \cdot 10^{-6})^{0.56} \cdot (N^2_{(i)})^{-0.43}$$

The Brunt-Väisälä buoyancy frequency is first determined as:

$$N^2_{(i)} = -\frac{g}{\rho_i} \cdot \frac{(\rho_i - \rho_{(i+1)})}{\Delta z}$$

Where **g** is the gravitational acceleration constant (9.80665 m s^{-2}), **ρ** is the water density (g cm^{-3}) and Δz is depth (distance) between the centroids of layers *i* and *i*+1 (m).

We determine the water density from Kalff (2002) as:

$$\rho_{(i)} = 1 - 6.63 \cdot 10^{-6} \cdot (temp_i - 4)^2$$

As an alternative and more complex approach, the vertical turbulent diffusivity, $\mathbf{K_{v(i)}}$, may also be read in from external file, and can thereby be based directly on a more complex physical model such as the General Ocean Turbulence Model (GOTM), following the approach in Mziray et al. (2024) and Trolle and Nielsen (2024). This will of course require that a physical model has been set up for the system, and that this model gives a good representation of the vertical mixing dynamics.

Mixed-layer deepening

The deepening rate of the surface mixed layer ($\Delta Z_{mix}\,\Delta t^{-1}$; m h^{-1}) describes the velocity of the surface mixed-layer deepening in both directions; it is positive when the volume of the hypolimnion is decreasing and negative when the hypolimnetic volume is increasing (Staehr et al. 2012). By dividing the deepening rate by the height (h) of the discrete depth layers and multiplying by the oxygen concentration (O_2) gradient between two adjacent layers, we can estimate the flux of oxygen due to mixed-layer deepening (Dz, g O_2 m^{-3} h^{-1}):

$$D_{z(i)} = \frac{\Delta Z_{mix}}{\Delta t} \cdot \frac{(O_{2(i)} - O_{2(i+1)})}{h}$$

As in the approach in Giling et al. (2017), Dz is calculated and applied only for layers within the metalimnion (i.e. all layers from depth = Z_{mix} to depth =

Z_{meta_lower}, +/- layer height). We have implemented an option to set a user-defined minimum threshold for $\Delta Z_{mix}\,\Delta t^{-1}$, before including the flux of oxygen due to mixed-layer deepening. This is implemented in an attempt to prevent short-term surface-water microstratification inaccurately affecting estimates of Dz.

Calibration of model parameters

The metabolism model has been developed in Python, where the three model parameters: $\mathbf{P_{max}}$, $\boldsymbol{\alpha}$ and $\mathbf{R_{20}}$, are calibrated for each single layer for each single day. The model user can choose between a series of numerical integration approaches and time steps to solve the metabolism model, but the 4^{th} order Runge-Kutta approach with an integration time step of 0.5 hour is used by default. A differential evolution algorithm is used to optimize the model parameters, which will automatically compare sensor-based observations with the model estimated oxygen concentrations, and optimize the model fit to observations. The differential evolution algorithm seeks to minimize an objective function (by default set to the root-mean-squared-error) for each single layer and each single day, and the final GPP and ER estimates are extracted from the calibrated model. Models with several parameters, such as the metabolism model, can exhibit equifinality, where good fits to observed data can be achieved by several different parameter value combinations, some unrealistic (e.g., Appling et al. 2018). The model approach by WateriTech overcomes this by constraining model parameter optimization to realistic ranges, and also by allowing the option to run an ensemble of model parameterizations using different initial parameter seeds for the differential evolution algorithm. The mean and the variation in model parameterization and simulated metabolism can then be extracted. In practice, we have found that even though the metabolism model may exhibit some degree of equifinality, the controlled parameter search results in similar estimates of GPP and ER, and therefore the effect of running ensembles is somewhat limited.

Operationalization and post-processing

WaterWebTools integration

The entire model workflow is automated via the WaterWebTools platform, where sensor data is live-streamed and pre-processed according to the steps described previously, local weather data is also harvested, and the metabolism model is executed operationally for each 24-hour time period. Parameter bounds used by the differential evolution algorithm, applied when optimizing the metabolism model, are constrained to value-ranges reported

in the literature (e.g. Hanson et al. 2008; Martinsen et al. 2022, also see Appendix), which ensure that the calibrated model parameters are within naturally realistic ranges. The output from the model can be followed live via the WaterWebTools platform (as seen in example below), and the platform can also be used to look for long-term trends in the ecosystem's metabolism, and thereby whether the health of the ecosystem is undergoing change.

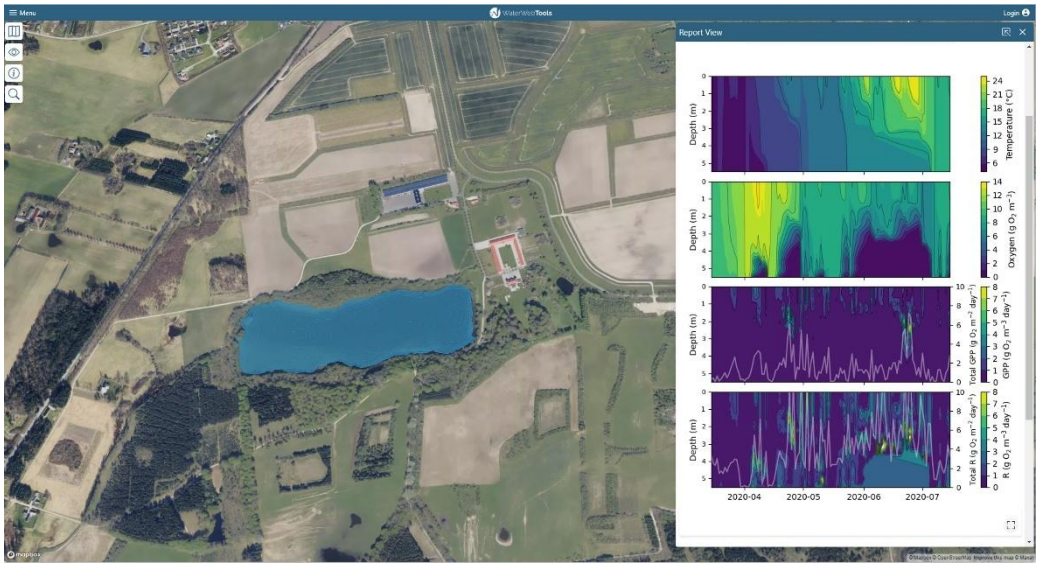

Fig. 2. Example of how oxygen and temperature profiles, and derived metabolism can be viewed within the WaterWebTools portal.

Metabolic fingerprint

If one or several years of metabolism data is available, we can also derive the metabolic fingerprint of the lake or fjord (Bernhardt et al. 2018). This represents the entire distribution of daily estimates of GPP and ER that are observed for a stream, lake or fjord, produced through kernel density plots, which allow visualization of peak metabolic rates, the most dominant combinations of GPP and ER, represented by centroid(s) of the metabolic fingerprint, as well as the variance in their ratio (Fig. 3).

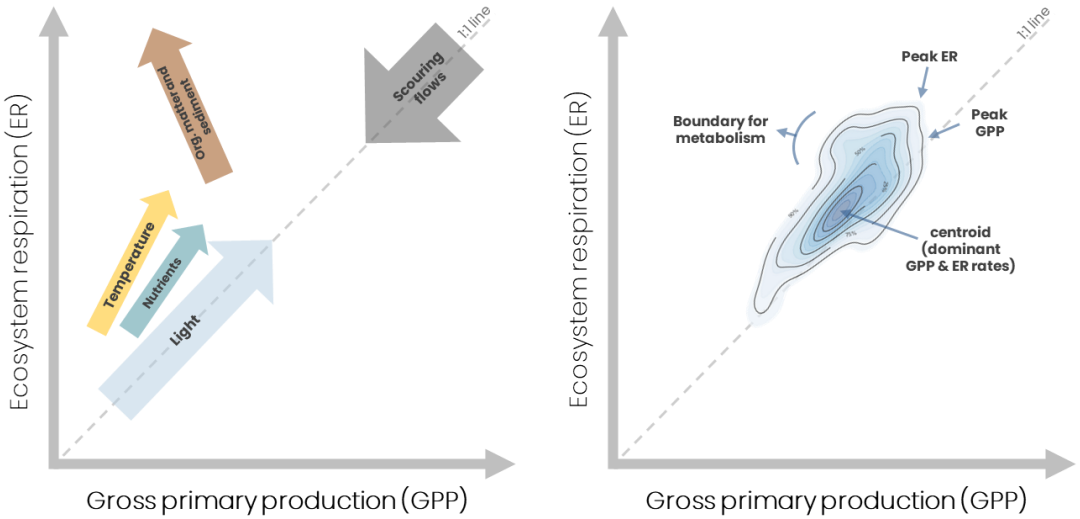

Fig. 3. The metabolic fingerprint (plot to the right) is a diagnostic tool first described by Bernhardt et al. (2018). It can be used for comparing annual patterns of metabolism across streams or across years for the same stream. The "fingerprint" is represented as a kernel density plot of daily estimates of GPP and R rates observed within the stream.

The metabolic fingerprint can be produced for each single year, and then used to follow long-term trajectories of the ecological balance of streams, helping us track changes that can signal stress or improvements in water quality. Is the river responding to improved upstream wastewater treatment, can we see any effects of implementing best-management-practices in nearby agriculture, or does restoration of floodplains or other nature-based-solutions have the expected benefits for the aquatic ecosystem? These are just some of the questions we can try to answer by keeping track of the metabolism.

References

Appling, A., Hall, R., Yackulic, C., Arroita, M. 2018. Overcoming Equifinality: Leveraging Long Time Series for Stream Metabolism Estimation. Journal of Geophysical Research: Biogeosciences, 123(2): 624-645. https://doi.org/10.1002/2017JG004140

Battin, T.J., Lauerwald, R., Bernhardt, E.S. et al. 2023. River ecosystem metabolism and carbon biogeochemistry in a changing world. Nature, 613 (7944): 449-459. https://doi.org/10.1038/s41586-022-05500-8

Bernhardt, E.S., Heffernan, J.B., Grimm, N.B., Stanley, E.H., Harvey, J.W., Arroita, M., Appling, A.P., Cohen, M.J., McDowell, W.H., Hall Jr, R.O. & Read, J.S., Roberts, B.J., Stets, E.G., Yackulic, C.B. 2018. The metabolic regimes of flowing waters. Limnology and Oceanography, 63: S99–S118, doi:10.1002/lno.10726

Caffrey, J.M. 2004. Factors Controlling Net Ecosystem Metabolism in U.S. Estuaries. Estuaries, 27: 90–101. https://doi.org/10.1007/BF02803563

Cole, J.J., Caraco, N.F. 1998. Atmospheric exchange of carbon dioxide in a low-wind oligotrophic lake measured by the addition of SF6. Limnology & Oceanography, 43(4): 647-656. https://doi.org/10.4319/lo.1998.43.4.0647

Crusies, J., Wanninkhof, R. 2003. Gas transfer velocities measured at low wind speed over a lake. Limnology & Oceanography, 48(3): 1010-1017. https://doi.org/10.4319/lo.2003.48.3.1010

Giling, D.P., Staehr, P.A., Grossart, H.P., Andersen, M.R., Boehrer, B., Escot, C., Evrendilek, F., Gómez-Gener, L., Honti, M., Jones, I.D., Karakaya, N., Laas, A., Moreno-Ostos, E., Rinke, K., Scharfenberger, U., Schmidt, S.R., Weber, M., Woolway, R.I., Zwart, J.A. and Obrador, B. 2017. Delving deeper: metabolic processes in the metalimnion of stratified lakes. Limnology and Oceanography, 62 (3): 1288-1306. https://doi:10.1002/lno.10504

Hanson, P.C., Carpenter, S.R., Kimura, N., Wu, C., Cornelius, S.P., Kratz, T.K. 2018. Evaluation of metabolism models for free-water dissolved oxygen methods in lakes. Limnol. Oceanogr.: Methods 6: 454–465.

Hall, R.O., Hotchkiss, E.R. 2017. Stream Metabolism. Chapter 34 in Methods in Stream Ecology. http://dx.doi.org/10.1016/B978-0-12-813047-6.00012-7

Hoellein, T.J., Bruesewitz, D.A., Richardson, D.C. 2013. Revisiting Odum (1956): A synthesis of aquatic ecosystem metabolism. Limnology and Oceanography, 58(6): 2089–2100. https://doi:10.4319/lo.2013.58.6.2089

Hondzo, M., Stefan, H.G. 1993. Lake water temperature simulation model. J. Hydraul. Eng. ASCE 119: 1251–1273, doi:10.1061/(ASCE)0733-9429(1993)119:11(1251)

Jankowski, K. J., Mejia, F., Blaszczak, J. R., & Holtgrieve, G. W. 2021. Aquatic ecosystem metabolism as a tool in environmental management. WIREs Water, 8(4). https://doi.org/10.1002/wat2.1521

Jørgensen, S.E. and Bendoricchio, B. (Eds.). 2001. Fundamentals of ecological modelling, 3rd ed. Developments in environmental modelling. V. 21. Elsevier.

Kalff, J., 2002. Limnology: inland water ecosystems, 1st ed. Prentice Hall, New Jersey.

Martinsen, K.T., Zak, N.B., Baastrup-Spohr, L., Kragh, T., Sand-Jensen, K. 2022. Ecosystem metabolism and gradients of temperature, oxygen and dissolved inorganic carbon in the littoral zone of a macrophyte dominated lake. Journal of Geophysical Research: Biogeosciences, 127(12), Article e2022JG007193. https://doi.org/10.1029/2022JG007193

Mziray, P., Stæhr, P.A., Christensen, J.P.A., Kimirei, I.A., Lugomela, C.V., Trolle, D., O'Reilly, C.M. 2024. Ecosystem metabolism in the deep and oligotrophic Lake Tanganyika. Journal of Great Lakes Research. https://doi.org/10.1016/j.jglr.2024.102337

Obrador, B., Staehr, P.A., Christensen, J.P.C. 2014. Vertical patterns of metabolism in three contrasting stratified lakes. Limnology and Oceanography, 59(4): 1228–1240. https://doi:10.4319/lo.2014.59.4.1228

Raymond, P.A., Zappa, C.J., Butman, D., Bott, T.L., Potter, J., Mulholland, P., Laursen, A.E., McDowell, W.H., Newbold, D. 2012. Scaling the gas transfer velocity and hydraulic geometry in streams and small rivers. Limnology and Oceanography: Fluids and Environments, 2: 41–53. https://doi.org/10.1215/21573689-1597669

Schilder, J., Bastviken, D., van Hardenbroek, M., Heiri, O. 2016. Spatiotemporal patterns in methane flux and gas transfer velocity at low wind speeds: Implications for upscaling studies on small lakes, J. Geophys. Res. Biogeosci., 121: 1456–1467, https://doi:10.1002/2016JG003346

Solomon, C.T., Bruesewitz, D.A., Richardson, D.C. et al. 2013. Ecosystem respiration: Drivers of daily variability and background respiration in lakes

around the globe. Limnology and Oceanography, 58(3), 849-866. https://doi.org/10.4319/lo.2013.58.3.0849

Song, C., Dodds, W.K., Trentman, M.T., Rüegg, J., Ballantyne, F. 2016. Methods of approximation influence aquatic ecosystem metabolism estimates. Limnol. Oceanogr. Methods 14: 557–569. https://doi:10.1002/lom3.10112

Staehr, P.A., Christensen, J.P., Batt, R.D., Read, J.S. 2012. Ecosystem metabolism in a stratified lake. Limnology and Oceanography, 57(5): 1317–1330. https://doi:10.4319/lo.2012.57.5.1317

Trolle, D., Nielsen, A. 2024. Sundhedstjek af søer, vandløb og fjorde via deres metabolisme. Aktuel Naturvidenskab (Danish popular science journal). https://aktuelnaturvidenskab.dk/find-artikel/nyeste-numre/5-2024/sundhedstjek-af-soeer-vandloeb-og-fjorde-via-deres-metabolisme

Vachon, D., Prairie, Y.T. 2013. The ecosystem size and shape dependence of gas transfer velocity versus wind speed relationships in lakes. Can. J. Fish. Aquat. Sci. 70: 1757–1764. https://doi:10.1139/cjfas-2013-0241

van't Veen, S.G.M., Kronvang, B., Audet, J. et al. 2025. SentemQC - A novel and cost-efficient method for quality assurance and quality control of high-resolution frequency sensor data in fresh waters. Open Res Europe, 4: 244 https://doi.org/10.12688/openreseurope.18134.1

Wilson, H.L., Ayala, A.I., Jones, I.D., Rolston, A., Pierson, D., de Eyto, E., Grossart, H.-P., Perga, M.-E., Woolway, R.I., Jennings, E. 2020. Variability in epilimnion depth estimations in lakes, Hydrol. Earth Syst. Sci. 24: 5559–5577, https://doi.org/10.5194/hess-24-5559-2020

Xu, W., Collingsworth, P.D., Minsker, B. 2019. Algorithmic characterization of lake stratification and deep chlorophyll layers from depth profiling water quality data. Water Resources Research, 55:3815–3834. https://doi.org/10.1029/2018WR023975

Appendix

Parameter bounds

Parameter bounds used when running the differential evolution algorithm have been derived from a review of metabolism studies, thereby ensuring that calibrated parameters are within naturally realistic ranges.

Parameter	Unit	Min.	Max.	References
P_{max}	g O_2 m^{-3} h^{-1}	0.001	2.1	Hanson et al. (2008), table 2 min. P_{max} = 0.004, max. P_{max} = 2.08
α	g O_2 m^{-3} h^{-1} [µmol photons m^{-2} s^{-1}]$^{-1}$	0.001	0.01	Obrador et al. (2014), page 1236 min. α = 0.004, max. α = 0.0096
R_{20}	g O_2 m^{-3} h^{-1}	0.001	1.75	Solomon et al. (2013), Fig. 7 min. R_{20} = 0, max. R_{20} = 0.625 Martinsen et al. 2022 (Fig 8) min. R_{20} = 0, max. R_{20} = 0.80 Assuming that R_{20} ~ 85% of P_{max} (ratio derived from Song et al. (2016), table A1) min. R_{20} = 0, max. R_{20} = 1.75